Soft Matter

Accepted Manuscript

ROYAL SOCIETY OF CHEMISTRY

www.rsc.org/softmatter

Soft Matter

ARTICLE

Migration of phospholipid vesicles in response to OH^- stimuli

Atsuji Kodama,[a] Yuka Sakuma,[a] Masayuki Imai,*[a] Yutaka Oya,[a] Toshihiro Kawakatsu,[a] Nicolas Puff,[bc] and Miglena I. Angelova,[bc]

Received 00th January 20xx,
Accepted 00th January 20xx

DOI: 10.1039/x0xx00000x

www.rsc.org/

We demonstrate a migration of phospholipid vesicles in response to pH gradient. Upon simple micro-injection of a NaOH solution, the vesicles linearly moved to the tip of the micro-pipette and the migration velocity was proportional to the gradient of OH^- concentration. The vesicle migration was characteristic of OH^- ions and no migration was observed for monovalent salts or nonionic sucrose solutions. The migration of vesicles is quantitatively described by the surface tension gradient model where the hydrolysis of the phospholipids by NaOH solution decreases the surface tension of the vesicle. The vesicles move toward a direction where the surface energy decreases. Thus the chemical modification of lipids produces a mechanical force to drive vesicles.

1 Introduction

The migration of vesicles in response to the concentration gradient of solutes is an essential characteristic of transport of vesicles in biological systems.[1,2] The motion of particles in the presence of the concentration gradient has been well described by the flow in the particle/fluid interfacial region.[3] When the particles have fluid nature, the surface tension gradient caused by the concentration gradient generates a unidirectional flow at the particle surface, which drives the particle, *i.e.*, "Marangoni effects".[4] For solid particles, interactions between the particle surface and solutes cause a flow in the interfacial region, which governs the motion, *i.e.*, "diffusiophoresis".[5,6] This difference originates from the fluidity of the particle.[3] In the case of vesicles, the internal fluid is enclosed by an incompressible 2D fluid membrane, which suppresses the unidirectional flow at the vesicle surface. Thus, even in the presence of the concentration gradient, vesicles behave as solid particles unless a symmetry breaking takes place in the flow of the lipid on the vesicle surface[7] and the dynamics should be governed by the diffusiophoresis mechanism, *i.e.*, interactions between the membrane and solutes.

It has been reported that the concentration gradient of solutes affects the vesicle dynamics[8-14]. When pH gradient is applied to anionic phospholipid vesicles fixed on a Pt wire, the vesicle membrane forms tubes, where the growth direction of the tube is determined by the value of pH.[11,12] The observed membrane deformation is well described by changes of the equilibrium lipid density and the spontaneous membrane curvature induced by the chemical modification of lipids in the outer leaflet.[12] By applying pH stimuli to fatty acid (decanoic acid/decanoate) vesicles, two types of unique response dynamics caused by solubilization of decanoate molecules are observed; deformations and topological transitions.[14] These observations strongly indicate that interactions between amphiphilic membranes and hydrogen ions/hydroxide ions govern the vesicle dynamics.

In this study we show the migration of neutral phospholipid vesicles in response to the pH gradient. By a micro-injection of NaOH solution to the free vesicles, the vesicles moved toward the source. First we examine the vesicle migration based on the diffusiophoresis mechanism and show that the diffusiophoresis is not responsible for the observed migration. As a control experiment of the vesicle migration, we examined response of spherical polystyrene particles to the pH gradient. The migration of polystyrene particles is well described by the diffusiophoresis mechanism. Then we present a surface tension gradient model, where we focus on chemical modifications of phospholipids by hydroxide ions. This observation shed light on the mechanism of vesicle transport driven by the concentration gradient of solutes.

2 Materials and methods

2.1 Chemicals

Synthetic neutral phospholipids, 1,2-dioleoyl-*sn*-glycero-3-phosphocholine (DOPC; purity > 99%) purchased from NOF CORPORATION (Tokyo, Japan) and 1,2-dipalmitoyl-*sn*-glycero-3-phosphocholine (DPPC; purity > 99%) purchased from Avanti Polar Lipids Inc. (Alabaster, USA) were used to prepare the giant vesicles (GVs) without further purification. The GVs were labeled by a fluorescent phospholipid, 1,2-dioleoyl-*sn*-glycero-3-phosphoethanolamine-N-(lissamine rhodamine B sulfonyl)

[a] Department of Physics, Tohoku University, Aoba, Sendai 980-8578, Japan.
[b] Laboratoire Matière et Systèmes Complexes, University Paris Diderot - Paris 7, F-75013 Paris, France.
[c] Faculty of Physics, University Pierre & Marie Curie - Paris 6, F-75005 Paris, France.
† Electronic Supplementary Information (ESI) available: Videos of migrations of phospholipid vesicles in response to pH gradient. See DOI: 10.1039/x0xx00000x

(Rh-DOPE) purchased from Avanti Polar Lipids Inc. (Alabaster, USA). We confirmed that the fluorescent label, Rh-DOPE (0.125 mol % to the total lipid) does not affect observed vesicle dynamics by a control experiment without Rh-DOPE. The polystyrene particles with a radius of R_c = 1.5 μm purchased from Magsphere Inc. (Pasadena, USA) were used after dialysis using cellulose tubes with the pore size ~ 50 Å (Viskase Companies Inc., Darien, USA). In the micro-injection experiments, the following chemicals were used; sodium hydroxide (NaOH), potassium hydroxide (KOH), hydrogen chloride (HCl), sodium chloride (NaCl), potassium chloride (KCl), and sucrose. All these chemicals in special grade were purchased from Wako Pure Chemicals Industries (Osaka, Japan). HEPES, 4-(2-hydroxyethyl)-1-piperazineethanesulfonic acid, purchased from DOJINDO LABOLATORIES (Kumamoto, Japan) was used for the preparation of supported lipid bilayers (SLBs) for contact angle measurements.

2.2 Preparation of giant vesicles

GVs composed of DOPC were prepared using a gentle hydration technique.[15,16] First, we mixed 100 μl of a chloroform solution of DOPC (10 mM) and 16.5 μl of a chloroform solution of Rh-DOPE (0.1 mg/ml) in a test tube. Then, we evaporated the organic solvent using a rotary evaporator N-1000 (Tokyo Rikakikai, Japan) at 50°C to produce homogeneous lipid films. After the evaporation, the test tube was put under a vacuum for 1 day to ensure the complete removal of the solvent. The pre-warmed lipid film was hydrated with 10 ml of pure water at 50 °C for 12 hours, which resulted in the formation of GVs with radii of 5 – 30 μm. The purified water was obtained from Direct-Q 3 UV system (Millipore, USA). All micro-injection experiments were performed within 1 day after the sample preparation. Just before we started micro-injection experiments, the pH value of the vesicle suspension was 6.5 – 6.1 at 25 °C.

2.3 Micro-injection experiments

The sample chamber for the micro-injection experiments was a hole in a silicone rubber sheet, which was placed onto a glass slide (Fig. 1). The hole had a diameter of 9 mm and a thickness of 1 mm. The micro-pipette used for the micro-injection was a Femtotips II with an inner diameter of 0.5 μm ± 0.2 μm (Eppendorf, Germany). To minimize the variation in the pipette diameter, we screened the pipettes by examining the injection flow with eye. After the screening, the variation in migration velocity of test colloid particles was controlled within ± 10%, which indicates the error caused by the variation in the pipette diameter is less than ± 10%. This error affects the concentration profile of the micro-injection. The positioning of the micro-pipette was controlled using a hydraulic micro-manipulator MMO-202ND (Narishige, Japan), and the micro-injection was performed using a Femtojet system (Eppendorf, Germany). The vesicle suspension was carefully transferred into the sample chamber from the test tube at room temperature. The micro-pipette filled with the injection solution was then inserted into the chamber. To minimize the drift flow in the sample solution, we carefully performed all procedures and waited for 10 min to equilibrate the sample. In addition, to avoid the effect of the flow generated by the evaporation we positioned the micro-pipette about 500 μm below the water surface, where no significant flow was observed. Then the distance from the tip of the injection pipette to the chamber bottom was about 500 μm, which is large enough compared with the size of experiment system, typically ~30 μm. Thus the observed vesicles were completely free from the bottom. The most of the injection experiments were performed with an injection pressure of 5 hPa, and the GV migration induced by the injection were observed using an

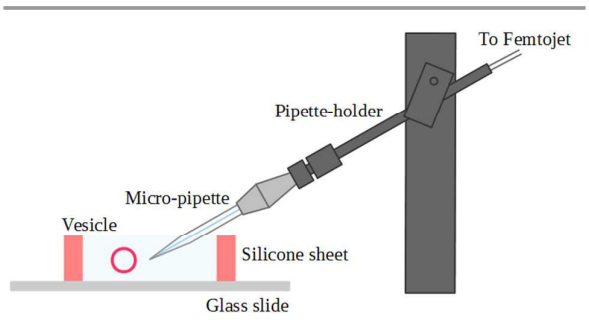

Fig. 1 Schematic representation of experiment setup for micro-injection.

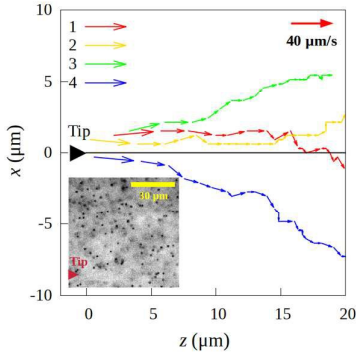

Fig. 2 Traces of colloid motion induced by the micro-injection with 5 hPa. Inset shows the distribution of colloids around the tip of the micro-pipette (triangle) before the injection.

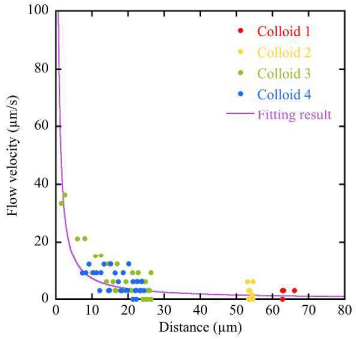

Fig. 3 Injection flow velocity, v, as a function of the distance between the tip and colloids. A solid line indicates the fitting function.

Axio Observer.Z1 inverted fluorescent microscope (Carl Zeiss, Germany) with a 20× objective (Plan-Neofluar 20× N.A. = 0.50) and recorded using a CCD camera, AxioCam MRm with the time resolution of 200 msec (Carl Zeiss, Germany) or a CMOS camera, ORCA-Flash 4.0 with the time resolution of 50 msec (Hamamatsu Photonics, Japan).

2.4 Effect of micro-injection flow on velocity of migrating vesicle

To obtain velocity of migrating vesicles, we have to correct a contribution of a flow generated by the micro-injection. We estimated the injection flow as follows. First we visualized the injection flow using colloids (diameter of 3 μm) dispersed in the medium (inset of Fig. 2) and estimated the velocity of the injection flow around the tip of the micro-pipette. Figure 2 shows traces of colloid motions induced by the micro-injection (length and direction of an arrow indicate the velocity of the colloid). Here it should be noted that the effect of gravity (terminal velocity ≅ 0.28 μm/s) on the injection flow velocity is too small to affect the horizontal component of the colloid flow velocity, typically about 10 μm/s. Since in the migration experiment we measured the velocities of the vesicles on the pipette axis (solid line in Fig. 2), we plot the z component of the velocity of the injection flow on the axis as a function of the distance between the colloid and the tip (Fig. 3). The flow velocity $\boldsymbol{v}(\boldsymbol{s},t)$ at position $\boldsymbol{s}$ (relative to the tip) and time t exerted by the external force $\boldsymbol{g}(\boldsymbol{s},t)$ is expressed as

$$\boldsymbol{v}(\boldsymbol{s},t) = \int d\boldsymbol{s}' \boldsymbol{\Omega}(\boldsymbol{s}-\boldsymbol{s}')\rho \boldsymbol{g}(\boldsymbol{s}',t) \quad (1)$$

$$\boldsymbol{\Omega}(\boldsymbol{s}) = \frac{1}{8\pi\eta s}\left(\boldsymbol{1}+\frac{\boldsymbol{ss}}{s^2}\right), \quad (2)$$

where ρ is the density of the fluid, η is the viscosity of the fluid, s is the magnitude of $\boldsymbol{s}$, $\boldsymbol{1}$ is the unit tensor, and $\boldsymbol{ss}$ is the dyadic product. Then we fit the observed distance dependence of the injection flow velocity using an inversely proportional function and obtained an expression, v = 72.12(±4.63)/s μm/s as shown in Fig. 3. This fitting function represents the injection flow velocity. By subtracting the contribution of the injection flow from the observed migration velocity, we obtained the corrected velocity of vesicle migration.

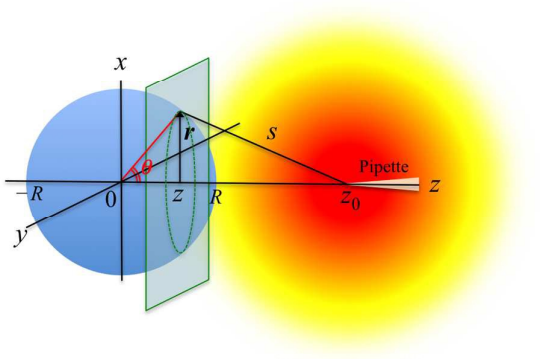

Fig. 4 Geometry of the micro-injection experiment. We injected NaOH solution at (0, 0, z_0), where the origin (0, 0, 0) is the position of the center of the spherical vesicle with a radius of R. The vesicle membrane with the shortest distance from the tip is located at (0, 0, R).

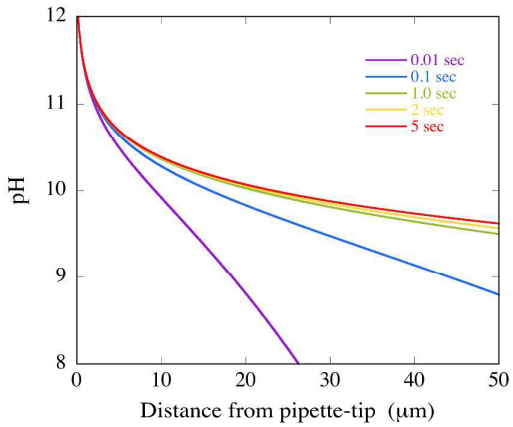

Fig. 5 Time evolution of the pH profile after the micro-injection of a 10 mM NaOH solution calculated using eqn. (3) with D_{OH^-}=5.27 × 10^{-9} m^2/s, S_0 = 4.3 × 10^{-19} mol/m^2s and ε = 0.25 × 10^{-6} m.

2.5 Concentration profile of OH^- ions around tip of micro-pipette

To estimate the concentration profile of OH^- ions around the tip of the micro-pipette, we calculated a time evolution of the concentration profiles by solving the diffusion equation with convoluting the inner radius of the pipette, ε, as

$$C_\infty(x,y,z,t) = \int_0^t \int_0^\varepsilon \int_0^{2\pi} \frac{S_0 \exp\left[-\frac{(x-\xi\cos\chi)^2+(y-\xi\sin\chi)^2+(z-z_0)^2}{4D(t-\tau)}\right]}{[4\pi D(t-\tau)]^{3/2}} \xi d\xi d\chi d\tau, \quad (3)$$

where S_0 is the flux of the injected solute from the pipette, D is the diffusion coefficient of the solute, and ξ and χ (polar coordinate) designate the position in the pipette mouth. The geometry of the micro-injection experiment is shown in Fig. 4. For micro-injection of 10 mM NaOH, we calculated the time dependence of the OH^- concentration profiles using D_{OH^-} = 5.27 × 10^{-9} m^2/s, S_0 = 4.3 × 10^{-19} mol/m^2s and ε = 0.25 × 10^{-6} m as shown in Fig. 5.[17] The concentration profile reaches to the steady one at ~ 1.0 sec. Since it took ~ 1.0 sec to start the migration of vesicles after the micro-injection, we expressed the OH^- concentration profile around the tip of the pipette by the steady state solution,

$$C_\infty^{OH}(x,y,z) = \frac{S_0}{4\pi D_{OH}} \int_0^\varepsilon \int_0^{2\pi} \frac{\xi d\xi d\chi}{\sqrt{(x-\xi\cos\chi)^2+(y-\xi\sin\chi)^2+(z-z_0)^2}}. \quad (4)$$

We estimated the effect of the variation in the pipette diameter on the concentration profile using eqn. (4).

2.6 Effects of pH on ζ potential and surface tension of DOPC membrane

To examine physical basis of the observed migration velocity of the vesicle, we estimated the effects of pH on the ζ potential and the surface tension of DOPC membrane. The ζ potential of DOPC vesicle was measured by using a zeta-potential analyzer, ELSZ-1000 (Otsuka electronics, Japan). For the ζ potential

measurements we prepared large unilamellar vesicles (LUVs). A thin film of DOPC (4 mg) on the walls of a glass vial was dried overnight under vacuum following the removal of the organic solvent under a nitrogen gas stream. The dried lipid film was rehydrated in a pure water to a concentration of 1 mg lipids/ml, resulting in the formation of multi-lamellar vesicles (MLVs). The MLVs were extruded 21 times through a polycarbonate filter with 100 nm pores using a extruder, Avanti Mini-Extruder purchased from Avanti Polar Lipids Inc. (Alabaster, USA) to prepare LUVs. The LUV suspension was diluted with NaOH solution for the ζ potential measurement at a desired concentration of NaOH.

The surface tension of DOPC membrane was estimated by contact angle measurements. We prepared the SLB using a standard vesicle fusion technique[18-21]. At first we prepared MLVs by rehydration of the DOPC dried film (4 mg) with 10 ml of a buffer solution (HEPES 10 mM, NaCl 50 mM, pH = 7.3). The obtained MLVs were sonicated using a probe sonicator (Branson) for 3 min at 22.5 kHz to obtain small unilamellar vesicles (SUVs). The SUV suspension was spread over the clean hydrophilic glass slide that was carefully washed in KOH solution and ultrapure water before dropping the suspension. Incubation for about 30 min at room temperature results in the formation of a SLB. The unfused vesicles were removed by washing with ultrapure water and then we annealed the SLB at 60 °C for 15 min to remove the excess water. We set a drop of NaOH solution with various pH values on the SLB. The contact angle was measured by a contact angle meter, DM-501 (Kyowa Interface Science, Japan).

3. Results and Discussion

3.1 Migration of vesicles triggered by NaOH micro-injection

The response of vesicles to the micro-injection of NaOH (10 mM, pH 12) is shown in Fig. 6 (video S1 in the ESI†). Spherical GVs with various radii (3 – 10 μm) and small lipid assemblies were homogeneously distributed in the vesicle suspension. The micro-pipette was carefully positioned in the suspension, and the NaOH solution was injected through the pipette. Here we continued the micro-injection during the observation (typically ~ 30 s). After the start of the injection (0.0 s), the small lipid assemblies (marked by dark blue arrowheads) near the micro-pipette moved to the tip (marked by a green arrowhead). After a certain time (~ 1 s), the GVs (marked by magenta, cyan and yellow arrowheads) at a distance of ~ 30 μm from the tip also began to migrate. The GVs linearly moved toward the tip with a velocity of several μm/s (4.0 – 22.0 s). With the elapse of time, GVs that were out of the field, which included the out-of-focal plane, were drawn to the tip (the vesicle marked by an orange arrowhead in 22.0 s frame). After reaching the tip, the GVs were stacked at the tip (24.0 and 25.0 s). This vesicle migration was sensitive to the concentration gradient of NaOH around the vesicle. When we stopped the injection, the motion of the vesicles stopped within 1 sec; when we restarted the injection, the vesicles resumed the migration toward the tip within 1 sec. In addition, for the micro-injection of a NaOH solution with a concentration of 1 mM or less (pH < 11), no migration of GVs was observed. Thus the migration has a pH threshold. Another important observation was chemical selectivity. We micro-injected various 10 mM chemical species: 1) basic solutions, NaOH and

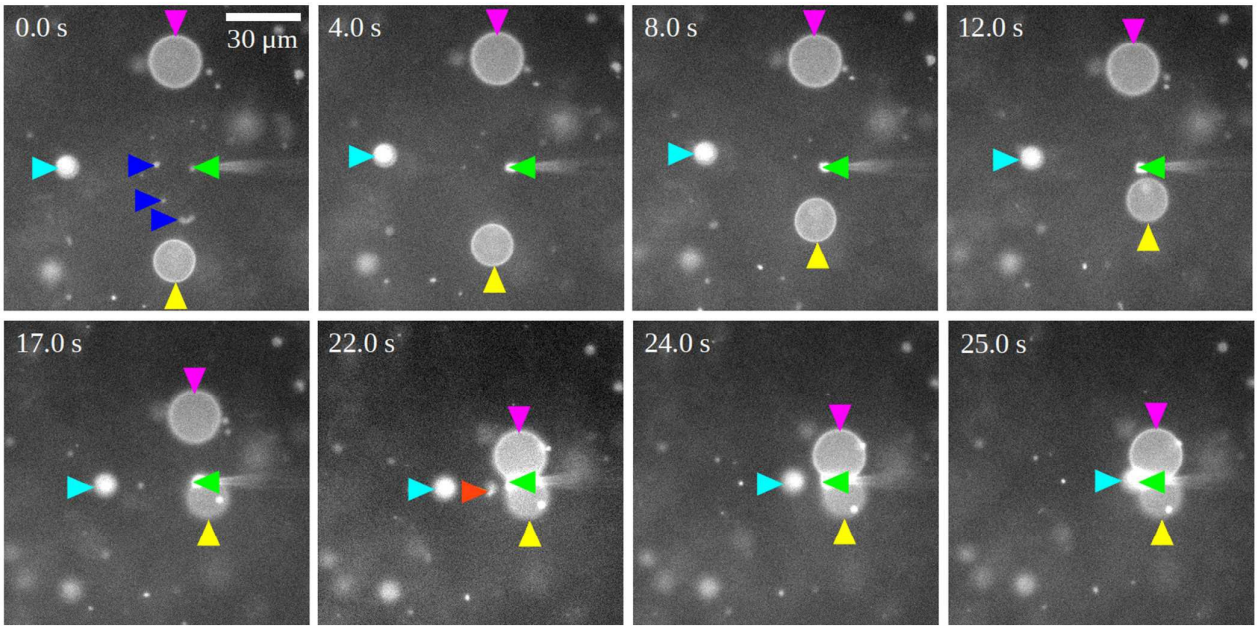

Fig. 6 Snapshot images of migrating GVs triggered by the micro-injection of a 10 mM NaOH solution. The elapsed time since the start of the micro-injection (t = 0.0 s) is shown at the top corner of each image. The representative GVs are marked with magenta, cyan, and yellow arrowheads in each image, and the tip of the micro-pipette is also marked with a green arrowhead. The small lipid assemblies near the micro-pipette are marked with dark blue arrowheads (0.0 s frame), and a GV from an out-of-focus plane is marked with an orange arrowhead (22.0 s frame). The scale bar in 0.0 s frame is 30 μm.

KOH; 2) an acidic solution, HCl; 3) monovalent salt solutions, NaCl and KCl; and 4) a nonionic solution, sucrose. The migration of vesicles was observed only for basic solutions, while no migration of vesicles toward the tip was observed for the injections of acidic, monovalent salt and sucrose solutions. A response of vesicles to the micro-injection of 10 mM NaCl solution is shown in video S2 in the ESI† as an example, where vesicles were flowed following the micro-injection flow. We concluded that the observed migration of vesicle is purely driven by the concentration gradient of the hydroxide ion.

3.2 Migration mechanism is neither Marangoni effect nor Diffusiophoresis

First we demonstrate that the migration is not driven by the unidirectional flow in the membrane, *i.e.*, Marangoni effect. To examine the flow in the vesicle membrane, we used phase separated vesicles composed of DOPC/DPPC = 6/4. In a state of rest the small domains show Brownian motion on the vesicle surface. By applying the pH gradient, the vesicle migrated toward the pipette tip, whereas the small domains on the vesicle continued the random motion, indicating that vesicles are not driven by Marangoni effect (video S3 in the ESI†). Then we focus on the diffusiophoresis as another possible mechanism to explain the observed vesicle migration. The effect of the OH^- stimuli on the behaviour of the phase separated vesicle is described in the ESI† S4.

The theory for the diffusiophoresis of spherical particles in electrolyte gradients is based on the electrokinetics,[6] where it assumes that the transport of ions is described by Nernst-Planck equation and the distribution of ions is governed by Poisson's equation, *i.e.*, no specific interaction between ions and membrane. For a symmetric electrolyte, $M^{+Z}X^{-Z}$, the migration velocity of a particle, U, expected by the diffusiophoresis mechanism is given by[6]

$$U = \frac{\varepsilon_r \varepsilon_0}{2\eta}\left(\frac{k_B T}{Ze}\right)^2 \left[u_0 + u_1 \lambda\right] \nabla \ln C_\infty \qquad (5)$$

$$\lambda = \frac{1}{\kappa R}, \qquad (6)$$

where ε_r and ε_0 are the dielectric constant of the fluid and the vacuum permittivity, respectively, k_B is Boltzmann's constant, T is the absolute temperature, e is the charge of an electron, C_∞ is the undisturbed electrolyte concentration, R is the radius of the particle and κ is the Debye screening length parameter expressed by

$$\kappa = \sqrt{\frac{\sum_i Z_i^2 e^2 C_\infty}{\varepsilon_r \varepsilon_0 k_B T}}. \qquad (7)$$

The u_0 is given by

$$u_0 = 2\beta \frac{Ze\zeta}{k_B T} - 4\ln(1-\gamma^2) \qquad (8)$$

with

$$\beta = \frac{D_+ - D_-}{D_+ + D_-} \qquad (9)$$

$$\gamma = \tanh\frac{Ze\zeta}{4k_B T}, \qquad (10)$$

where ζ is the ζ potential, D_+ and D_- are the diffusion coefficients of the cation and the anion, respectively. The first term in eqn. (8) stands for the "electrophoresis" mechanism which is based on the electric field due to the concentration gradient of the electrolyte, and the second term stands for the "chemiphoretic" mechanism which is analogous to the diffusiophoresis of nonelectrolytes. The u_1 is a complex function of ζ and β and expressed by

$$u_1 = F_0 + \beta F_1 + \frac{\varepsilon_r \varepsilon_0}{2\eta D}\left(\frac{k_B T}{Ze}\right)^2 \left[F_2 + \beta(F_3 + F_5) + \beta^2 F_4\right], \qquad (11)$$

where the values of F_n (n = 0 – 5) are evaluated numerically and tabulated in ref. 6.

To examine this diffusiophoresis mechanism, we measured

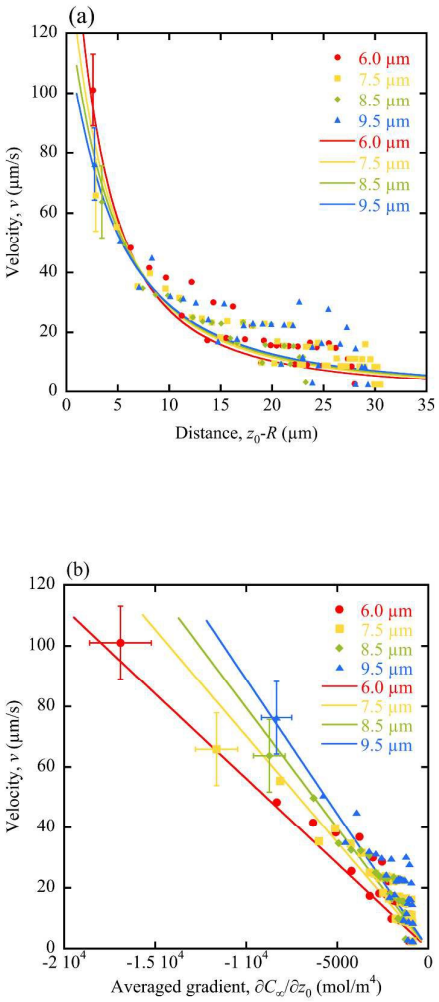

Fig. 7 Migration velocity of vesicles in response to micro-injection of 10 mM NaOH. (a) Variation in the velocity for the migrating GVs as a function of the distance from the tip of the micro-pipette. The radii of the GVs are 6.0 (red circle), 7.5 (orange square), 8.5 (green diamond), and 9.5 (blue triangle) μm. The solid line is a theoretical prediction based on the surface tension gradient model, eqn. (17). (b) The velocities are plotted against averaged concentration gradient. Error bars are indicated at highest velocity data for each vesicle. Error in velocity originates from the pixel size and error in averaged concentration gradient is due to the variation in the pipette diameter.

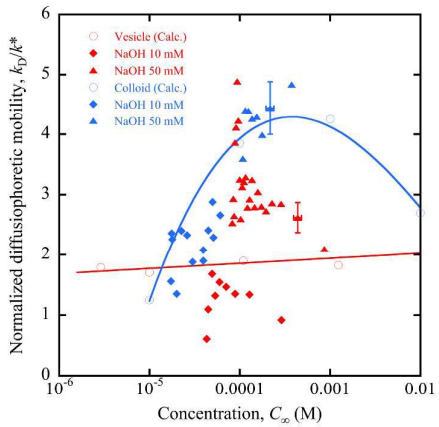

Fig. 8 Diffusiophoretic mobility of DOPC vesicles (red) and polystyrene colloids (blue) in response to micro-injection of 10 mM NaOH as a function of NaOH concentration. Closed symbols are experimental data (diamonds: 10 mM NaOH injection and triangles: 50 mM NaOH injection) and open symbols are theoretical predictions. The solid lines are interpolations connecting theoretical symbols. For convenience we showed error bars for typical data. Error in velocity originates from the pixel size and error in averaged concentration gradient is due to the variation in the pipette diameter.

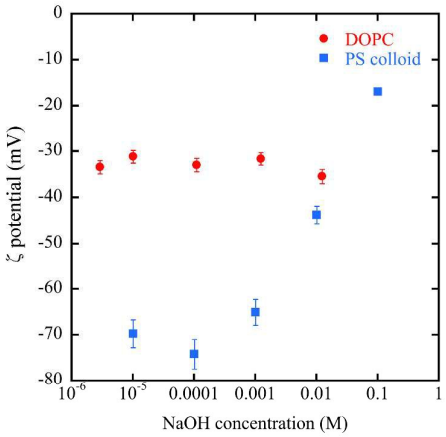

Fig. 9 Dependence of ζ potential of DOPC vesicle (red circle) and polystyrene colloid (blue square) on NaOH concentration.

velocities of migrating vesicles as a function of the distance from the tip of the micro-pipette. In the measurement we adopted the vesicles located on the pipette axis (z axis in Fig. 4). When the vesicles were subjected to the micro-injection, they linearly moved on the z axis toward the tip. Here the density of DOPC membrane is ~ 1.002 g/cm^3, which is close to the density of water. Then we ignored the effect of gravity on the vesicle motion during the migration (typical migration time is 2 - 5 sec). The corrected velocity profiles of the migrating GVs with radii ranging from 6.0 to 9.5 μm after injection of a 10 mM NaOH solution are plotted in Fig. 7(a). Here the distance means the shortest distance between the tip and the vesicle membrane. In this plot the data are scattered, e.g. 3 – 30 μm/s at the distance of about 25 μm. This is because the CMOS camera has the pixel size of 0.3 μm × 0.3 μm in the frame image and we took an image every 50 ms. The migration distance of the vesicle with the velocity of 15 μm/s during 50 ms is 0.75 μm. Taking into account the error to fix the center of the vesicle, the error to estimate vesicle velocity is 2 pixel/frame, i.e. 0.75 ± 0.6 μm/50 ms = 15 ± 12 μm/s. The velocity of the migrating vesicle exponentially increased as the GV approached the tip and reached to ~ 100 μm/s before it touched the pipette. From the observed migration velocity, v, we extracted the diffusiophoretic mobility, k_D, defined by

$$v = k_D \nabla \ln C_\infty \quad (12)$$

$$k_D = \frac{\varepsilon_r \varepsilon_0}{2\eta}\left(\frac{k_B T}{Ze}\right)^2 [u_0 + u_1 \lambda] \quad , \quad (13)$$

Here the concentration gradient, $\nabla \ln C_\infty$, at vesicle-tip distance $s = \sqrt{z_0^2 - 2Rz_0\cos\theta + R^2}$ is calculated by the solution of the diffusion equation at the steady state, eqn. (4). We plot the normalized diffusiophoretic mobility, k_D/k^*, [$k^* = (\varepsilon_r \varepsilon_0 / 2\eta)(k_B T / Ze)^2$] obtained by two experimental sets (micro-injections of 10 and 50 mM NaOH) as a function of NaOH concentration at the vesicle position (Fig. 8), where we use Z = 1, R = 10 × 10^{-6} m and η = 1 × 10^{-3} Pa s. Both experimental data have a sharp peak and do not overlap each other. The theoretical prediction of the diffusiophoretic mobility is calculated by using eqn. (5) – (11), where we measured the ζ potential as a function of NaOH concentraton and found that ζ (c.a. –32 mV) is negative[22-26] and independent of pH (Fig. 9). The theoretical diffusiophoretic mobility of DOPC vesicle using ζ = –32 mV, e = 1.60 × 10^{-19} C, ε_0 = 8.85 × 10^{-12} Fm^{-1}, ε_r = 80.4, β = –0.6 (D_{Na^+} =1.33 × 10^{-9} m^{2}s^{-1} and D_{OH^-} =5.27 × 10^{-9} m^{2}s^{-1}),[17] k_BT = 4.11 × 10^{-21} J, and R = 10 × 10^{-6} m, is plotted in Fig. 8. The theoretical prediction is almost independent of the concentration, which is completely different from the experimental data. As a counter experiment we examined migration of polystyrene particles triggered by the micro-injection of NaOH, since Ebel et al. reported that the migration of polystyrene particles in the concentration gradient of electrolyte is well described by the diffusiophoresis theory.[27] The experimental k_D/k^* data of the polystyrene particles for micro-injections of 10 and 50 mM NaOH are consistent with each other and increase with increasing in NaOH concentration as shown in Fig. 8. The theoretical diffusiophoretic mobility calculated by eqn. (5) – (11) agrees with the experimental k_D/k^* data, where the pH dependence of the ζ potential of polystyrene colloids is shown in Fig. 9. We can clearly demonstrate the difference in migration mechanism between the vesicles and the polystyrene particles by using a mixed sample. When we micro-injected 10 mM NaCl solution to the vesicle and the colloid located at ~ 30 μm apart from the tip, the colloid migrated toward the tip, whereas the vesicle went away slowly following the injection flow (video S5 in the ESI†). These experimental results suggest that the migration of vesicles in the pH gradient is not governed by the diffusiophoresis mechanism.

3.3 Effect of NaOH on DOPC membrane

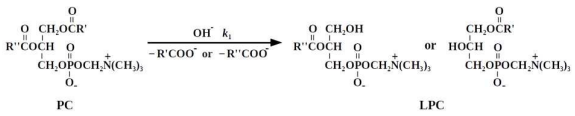

Fig. 10 A scheme of hydrolysis from phosphatidylcholine (PC) to lyso-phosphatidylcholine (LPC) at high pH condition.

A plausible reason to explain the difference between the observed migration of vesicles and the diffusiophoresis model might be a specific interaction between OH^- and membrane. It is well known that in the high pH region OH^- ions hydrolyze the glycerol group in the phosphatidylcholine,[28-33] where OH^- ions attack four ester bonds in a phospholipid molecule and the carboxy esters are hydrolysed faster than the phosphate ester.[33] A scheme of hydrolysis from phosphatidylcholine (PC) to lyso-phosphatidylcholine (LPC) and fatty acid (-R'COO^- or –R"COO^-) is shown in Fig. 10. The alkaline hydrolysis of phospholipids was quantified by using a gel chromatograph technique and the rate constants ranges from 0.1 to 20 s^{-1} M^{-1} depending on chain lengths (dipalmitoyl-, dimyristoyl-, and dilauroyl-phosphatidylcholine), type of head groups (phosphatidylcholine and phosphatidylethanolamine) and aggregation states (monomers, micelles, vesicles, and multibilayers).[29] In high pH region, DOPC produces 18:1-lyso-PC and oleic acid by the hydrolysis. The oleic acids form micelles at high pH region and the cac (critical aggregate concentration) of oleic acid/oleate vesicle is 0.4 – 0.7 mM.[34] Thus produced oleic acids in vesicles dissolve into water phase. Since LPC is more hydrophilic compared with PC, the surface tension of the membrane might decrease due to the hydrolysis, where the surface tension originates from the contact energy between the membrane surface and the NaOH solution. The effect of the hydrolysis of PC on the surface tension was examined by measuring the contact angle as shown in Fig. 11. In this experiment we waited 30 sec to start measuring the contact angle after we dropped the solution, since the contact angle decreased with time due to the progress of the hydrolysis. The observed contact angle, φ, kept a constant value (φ ~ 0.85 rad) in the pH range of 2 – 10 and decreased to φ ~ 0.18 at pH = 13, which strongly indicates that the hydrolysis at high pH region decreases the surface tension. We describe the details of the contact angle measurement in the ESI† S6. The vesicle senses pH gradient produced by micro-injection of NaOH solution with high pH, which causes the asymmetry of the surface tension between the front and the rear side of the vesicle. This asymmetry might drive the vesicle to decrease the surface energy. In addition we show that the dissociation of the head group due to the pH change is not responsible for the observed vesicle migration in the ESI† S7 .

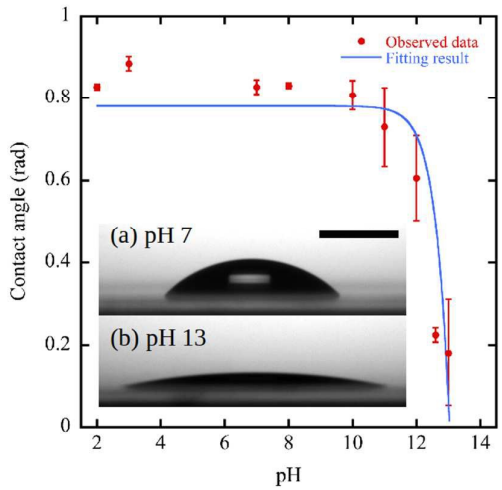

Fig. 11 pH dependence of contact angles of droplets on supported lipid bilayer. Insets (a) and (b) are snapshots of droplets with pH 7 and pH 13, respectively. The scale bar indicates 2 mm. The Observed data was fitted using a linear function as described in the ESI† S6.

3.4 Vesicle migration can be explained by surface tension gradient mechanism

The driving force caused by the surface tension gradient is expressed by

$$f(z_0,t)=\frac{\partial E(z_0,t)}{\partial z_0} \tag{14}$$

$$E(z_0,t)=\int_0^{\pi}\gamma(s,t)2\pi R^2\sin\theta d\theta\,, \tag{15}$$

where γ is the surface tension, and $E(z_0, t)$ is the total surface energy of the vesicle. The migration velocity of fluid particle with the internal viscosity $\bar{\eta}$ is given by[7]

$$v=\frac{(\eta+\bar{\eta})f}{2\pi\eta R(2\eta+3\bar{\eta})}=\frac{(\eta+\bar{\eta})R}{(2\eta+3\bar{\eta})\eta}\int_0^{\pi}\left(\frac{\partial\gamma}{\partial z_0}\right)\sin\theta d\theta\,. \tag{16}$$

For vesicles, the internal viscosity should be $\bar{\eta}\to\infty$.[7] Thus, even in the presence of the concentration gradient, vesicles behave as solid particles since the membrane is an incompressible 2D fluid. Then the velocity is given by

$$v=\frac{R}{3\eta}\int_0^{\pi}\left(\frac{\partial\gamma}{\partial z_0}\right)\sin\theta d\theta=\frac{R}{3\eta}\left(\frac{\partial\gamma}{\partial C_\infty}\right)\int_0^{\pi}\left(\frac{\partial C_\infty}{\partial z_0}\right)\sin\theta d\theta\,. \tag{17}$$

Since the surface tension is governed by the hydrolysis of the phospholipids, for convenience we expressed the surface tension by summing the contributions from PC and LPC as

$$\gamma=\gamma_0^{\mathrm{PC}}\frac{[\mathrm{PC}]}{[\mathrm{PC}]+[\mathrm{LPC}]}+\gamma_0^{\mathrm{LPC}}\frac{[\mathrm{LPC}]}{[\mathrm{PC}]+[\mathrm{LPC}]}\,, \tag{18}$$

where γ_0^{PC} and γ_0^{LPC} are the specific surface tension of DOPC and hydrolyzed DOPC, respectively, and $[\cdots]$ means the molar concentration in the membrane, *i.e.* $[\mathrm{PC}]_0 = [\mathrm{PC}] + [\mathrm{LPC}] = 3\times10^{-6}$ mol/m^2 ($[\mathrm{PC}]_0$: concentration of DOPC before the micro-injection).[35] The concentration of LPC is determined by a rate equation of the hydrolysis,

$$\frac{d[\mathrm{LPC}]}{dt}=k_1C_\infty^{\mathrm{OH}}[\mathrm{PC}], \tag{19}$$

where k_1 is the rate constant. Combining eqn. (18) and (19), we obtain

$$\begin{aligned}\gamma&=\gamma_0^{\mathrm{PC}}+\Delta\gamma_0(1-\exp(-k_1C_\infty^{\mathrm{OH}}t))\\&\simeq\gamma_0^{\mathrm{PC}}+\Delta\gamma_0k_1C_\infty^{\mathrm{OH}}t\end{aligned}\,, \tag{20}$$

where $\Delta\gamma_0=\gamma_0^{\mathrm{LPC}}-\gamma_0^{\mathrm{PC}}$. Then the surface tension gradient is given by

$$\frac{\partial \gamma}{\partial C_{\infty}^{\mathrm{OH}}} = \Delta\gamma_0 k_1 t \,. \qquad (21)$$

We estimated $\partial\gamma / \partial C_{\infty}^{\mathrm{OH}}$ in eqn. (21) from the concentration gradient of the contact angle, φ, (Fig. 11), using Young's equation,

, (22)

where γ_{lg} and γ_{mg} are the liquid/gas and membrane/gas surface tensions, respectively. Here we found that the γ_{lg} is independent of pH and has a value of about 73 mN/m (ESI† S6). Then we obtained a relationship

$$\frac{\partial \gamma}{\partial C_{\infty}^{\mathrm{OH}}} = \gamma_{\mathrm{lg}} \sin\varphi \frac{\partial \varphi}{\partial C_{\infty}^{\mathrm{OH}}} \,. \qquad (23)$$

Since the surface tension varies with time due to the hydrolysis, to calculate the velocity of the migrating vesicle by eqn. (17), we used the surface tension gradient induced by hydrolysis for 1 sec, *i.e.* $\partial\gamma / \partial C_{\infty}^{\mathrm{OH}} = \Delta\gamma_0 k_1$. By combining eqn. (21) and (23), we obtained $\Delta\gamma_0 k_1$ = −3.8 (±1.1) 10^{-3} N m^{-1} M^{-1} s^{-1}. The calculated migration velocities of vesicles with various radii are plotted in Fig. 7(a). Our model well describes observed migration velocity of the vesicles quantitatively. For reference we plot the velocity against the averaged concentration gradient in Fig. 7(b), which exhibits a linear relationship between the velocity and the concentration gradient as predicted by eqn. (17).

Here we interpret the observed pH threshold and chemical selectivity based on the surface tension gradient model. For the pH threshold, the key is that the migration velocity of the vesicle decreases with decreasing in the concentration of OH^-. When we micro-inject 1 mM NaOH (pH 11), the surface tension gradient model predicts the migration velocity of c.a. 0.5 μm/s at the distance of 30 μm, which is smaller than the injection flow velocity of c.a. 2 μm/s there. Thus we cannot observe the definite migration. The chemical selectivity might originate from the modification of the surface tension by chemicals. To examine the effect of chemicals on the surface tension, we measured contact angles of 10 mM NaCl, 10 mM sucrose droplets on the supported DOPC membrane. The observed contact angles of NaCl (0.87 ± 0.02 rad) and sucrose (0.82 ± 0.05 rad) had almost the same as that of pure water

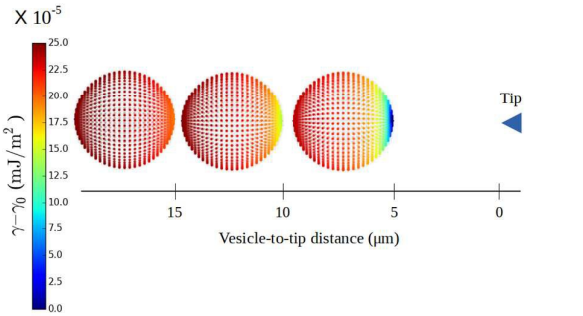

Fig. 12 The surface tension distribution on the vesicle membrane with R = 10 μm is visualized as a function of the vesicle-to-tip distance of 15, 10, and 5 μm when 10 mM NaOH solution is injected. The color bar indicates the scales for the difference interfacial energy densities, $\gamma - \gamma_0$ (mJ/m^2) with γ_0 = 1.9997 mJ/m^2.

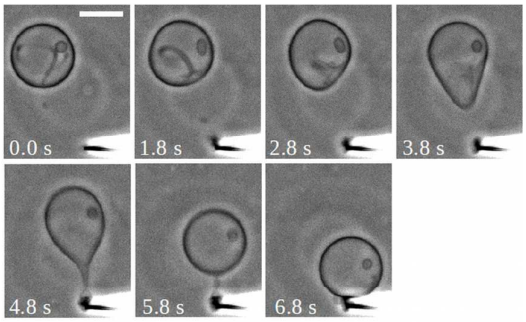

Fig. 13 Response of a GV with an invaginated tube subjected to micro-injection with a 10 mM NaOH solution. The elapsed time after the injection is shown in the figure. The scale bar indicates 20 μm.

(0.83 ± 0.01 rad), which indicates that the surface tension are independent of the concentration of NaCl and sucrose, *i.e.* $\partial\gamma/\partial C_{\infty} \sim 0$ (Fig. S5 in the ESI† S8). Thus for NaCl and sucrose the vesicles are not driven by the surface tension gradient. In this case the motion of vesicle in response to the pH gradient should be described by the diffusiophoresis mechanism. For the micro-injection of 10mM NaCl (electrolyte), the expected migration velocity by eqn. (5) – (11) with $\zeta \sim -30$ mV and D_{Cl^-} = 2.03 × 10^{-9} m^2/s is c.a. 4 μm/s at the distance of 30 μm, which is comparable to the injection flow velocity there. Thus the surface tension gradient model well explains observed features of the vesicle migration.

3.5 Deformation of vesicle coupled with migration

We visualized the surface tension distribution on the vesicle with R = 10 μm at the distance of 15, 10, and 5 μm using eqn. (20) as shown in Fig. 12. The surface tension distribution has a minimum at the front pole. This asymmetric distribution of the surface tension on a vesicle produces a pulling force, which drives the vesicle toward the tip. As the vesicle approaches the tip, the asymmetry of the surface tension increases, which results in the observed increase of the migration velocity. If the vesicle has an excess area, the pulling force causes not only the migration but also the shape deformation of the vesicle. Figure 13 shows the response of a GV with an invaginated tube to the micro-injection of a 10 mM NaOH solution (video S6 in the ESI† S9). Immediately after the micro-injection, the GV began moving, and simultaneously the membrane started to deform toward the tip. With the elapse of time, the vesicle membrane was stretched to the tip, which regressed the invaginated tube (1.8 and 2.8 sec). At 3.8 sec, the GV deformed to a teardrop shape without the invagination. From the apex of the teardrop vesicle, a tubular membrane was protruded toward the tip and bridged between the tip and the GV (4.8 sec). Because of the strong tension, the tube exhibited a pearling instability,[36] and the mother vesicle recovered the spherical shape (5.8 sec). Finally, the GV attached to the tip (6.8 sec). Here we estimated volume change of the vesicle due to the osmotic pressure difference caused by the micro-injection. When we micro-inject 10 mM NaOH solution to the vesicle located at 10 μm apart from the

tip of the micro-pipette, the vesicle feels the difference in molar concentration across the membrane, C ~ 1 mM (Fig. 5). The volume change ΔV during time Δt due to the osmotic difference is expressed by

$$\frac{\Delta V / v_m}{\Delta t} = -APC \,, \qquad (24)$$

where v_m is the water molar volume, A is the membrane surface area, P (= 4×10^{-3} cm s^{-1}) is the membrane permeability.[37] During the migration (~ 5 sec), the estimated volume change using eq. (24) is ~ 0.1 % at the most, which is too small to affect the vesicle deformation during the migration.

The observed shape deformation of the GV coupled with the migration indicates a strong pulling force. The pulling force that acts on the center of the vesicle at the distance, z_0 is calculated by eqn. (14) and (15) (Fig. S6 in the ESI† S10). The force acting on the vesicle increases exponentially as the vesicle approaches the tip and reaches 5 pN at the distance of 10 μm. This pulling force is consistent with the reported pulling force needed to protrude the tubular membrane from the mother vesicle.[38-40]

Conclusions

By applying pH gradient to phospholipid vesicles, they migrate toward the high pH region. In the case of vesicles, the internal fluid is enclosed by an incompressible 2D membrane, which suppresses a unidirectional flow in the membrane. Thus the Marangoni effect is not responsible for the observed migration of vesicles. Furthermore the observed migration of vesicle is not described by the diffusiophoresis mechanism. Here we propose a surface tension gradient model where a surface tension gradient produced by the hydrolysis of phospholipids drives the vesicle toward high pH region. This model well describes the observed behaviors; 1) migration velocity as a function of distance between the tip and the vesicle, 2) pH threshold for the migration, 3) the chemical selectivity, and 4) protrusion of vesicle toward the tip. To our knowledge this is the first report of the unidirectional vesicle migration triggered by the chemical modification of the vesicle membrane. The directed motion of vesicles within cells is an extremely important biological transport process, where vesicles move in response to very small gradients of chemical species. Our observations might shed light on the road to understanding vesicular transport systems in cells. For this purpose further systematic experimental work investigating the specific response of different lipid species to various chemical stimuli is currently in progress in our labs.

Acknowledgements

This work was supported by Grant-in-Aid for Scientific Research (A) 22244053, 25247070, Grant-in-Aid for Scientific Research on Innovative Areas ``Fluctuation & Structure'' (No. 25103009), and the Core-to-Core Program ``Non-equilibrium dynamics of soft matter and information'' from the Japan Society for the Promotion of Science.

References

1 J. L. Anderson, *Ann. NY Acad. Sci.*, 1986, **469**, 166.
2 R. D. Allen, *Sci. Am.*, 1987, **265**, 42.
3 J. L. Anderson, *Ann. Rev. Fluid Mech.*, 1989, **21**, 61.
4 N. O. Young, J. S. Goldstein, and M. J. Block, *J. Fluid Mech.*, 1959, **6**, 350.
5 J. L. Anderson, M. E. Lowell, and D. C. Prieve, *J. Fluid Mech.*, 1982, **117**, 107.
6 D. C. Prieve, J. L. Anderson, J. P. Ebel, and M. E. Lowell, *J. Fluid Mech.*, 1984, **148**, 247.
7 L. D. Landau, and E. M. Lifshitz, *Fluid Mechanics 2nd ed. Course of Theoretical Physics Vol 6*, Butterworth-Heinemann, Oxford, 1987.
8 I. Cantat and C. Misbah, *Phys. Rev. Lett.*, 1999, **83**, 235.
9 I. Cantat, K. Kasnner, and C. Misbash, *Eur. Phys. J. E*, 2003, **10**, 175.
10 T. Miura, H. Oosawa, M. Sakai, Y. Syundou, T. Ban, and A. Shioi, *Langmuir*, 2009, **26**, 1610.
11 N. Khalifat, N. Puff, B. Bonneau, J.-B. Fournier, and M. I. Angelova, *Biophys. J.*, 2008, **95**, 4924.
12 J.-B. Fournier, N. Khalifat, N. Puff, and M. I. Angelova, *Phys. Rev. Lett.*, 2009, **102**, 018102.
13 A. F. Bitbol, N. Puff, Y. Sakuma, M. Imai, J.-B. Fournier, and M. I. Angelova, *Soft Matter*, 2012, **8**, 6073.
14 K. Ikari, Y. Sakuma, T. Jimbo, A. Kodama, M. Imai, P.-A. Monnard, and S. Rasmussen, *Soft Matter*, 2015, **11**, 6327.
15 J. P. Reeves and R. M. Dowben, *J. Cell Physiol.*, 1969, **73**, 49.
16 K. Akashi, H. Miyata, H. Itoh, and K. J. Kinoshita, *Biophys. J.*, 1996, **71**, 3242.
17 E. L. Cussler, *Diffusion - Mass Transfer in Fluid Systems*, Cambridge University Press, Cambridge, 2009.
18 B. Sanii, A. M. Smith, R. Butti, A. M. Brozell, and A. N. Parikh, *Nano Lett.*, 2008, **8**, 866
19 J. S. Hovis and S. G. Boxer, *Langmuir*, 2000, **16**, 894.
20 A. B. Subramaniam, S. Lecuyer, K. S. Ramamurthi, R. Losick, and H. A. Stone, *Adv. Matter*, 2010, **22**, 2142.
21 M. Staykova, D. P. Holmes, C. Read, and H. A. Stone, Proc. *Natl. Acad. Sci.*, 2011, **108**, 9084.
22 S. A. Tatulian, *Biochim. Biophys. Acta*, 1983, **736**, 189.
23 S. Ohki, S. Roy, H. Ohshima, and K. Leonards, *Biochemistry*, 1984, **23**, 6126.
24 D. Papahadjopoulos, *Biochim. Biophys. Acta*, 1968, **163**, 240.
25 K. Makino, T. Yamada, M. Kimura, T. Oka, H. Ohshima, and T. Kondo, *Biophys. Chem.*, 1991, **41**, 175.
26 A. D. Petelska and Z. A. Fegaszewski, *Biophys. J.*, 2000, **78**, 812.
27 J. P. Ebel, J. L. Anderson, and D. C. Prieve, *Langmuir*, 1998, **4**, 396.
28 E. Baer and M. Kates, *J. Bio. Chem.*, 1950, **185**, 615.
29 C. R. Kensil and E. A. Dennis, *Biochemistry*, 1981, **20**, 6079.
30 M. A. Wells, *Biochemistry*, 1974, **13**, 2248.
31 R. J. Y. Ho, M. Schmetz, and D. W. Deamer, *Lipids*, 1987, **22**, 156.
32 M. Grit and D. J. Crommelin, *Chem. Phys. Lipids*, 1993, **64**, 3.
33 J. M. A. Kemps and D. J. A. Crommelin, *Pharm. Weekbl.*, 1988, **123**, 355.
34 K. Morigaki and P. Walde, *Curr. Opin. Colloid Interface Sci.*, 2007, **12**, 75.
35 J. F. Nagle and S. Tristram-Nagle, *Biochim. Biophys. Acta.*, 2000, **1469**, 159.
36 R. Bar-Ziv, E. Moses, and P. Nelson, *Biophys. J.*, 1998, **75**, 294.
37 E. Boroske, M. Elwenspoek, and E. Helfrich, *Biophys. J.*, 1981, **34**, 95.
38 I. Derényi, F. Julicher, and J. Prost, *Phys. Rev. Lett.*, 2002, **88**, 238101.

39 A. Upadhyaya and M. P. Sheetz, *Biophys. J.*, 2004, **86**, 2923.
40 D. Cuvelier, I. Derényi, P. Bassereau, and P. Nassoy, *Biophys. J.*, 2005, **88**, 2714.